Diffuse light and galaxy interactions in the core of nearby clusters

Magda Arnaboldi

Abstract The kinematics of the diffuse light in the densest regions of the nearby clusters can be unmasked using the planetary nebulae (PNs) as probes of the stellar motions. The position-velocity diagrams around the brightest cluster galaxies (BCGs) identify the relative contributions from the outer halos and the intracluster light (ICL), defined as the light radiated by the stars floating in the cluster potential. The kinematics of the ICL can then be used to asses the dynamical status of the nearby cluster cores and to infer their formation histories. The cores of the Virgo and Coma are observed to be far from equilibrium, with mergers currently ongoing, while the ICL properties in the Fornax and Hydra clusters show the presence of sub-components being accreted in their cores, but superposed to an otherwise relaxed population of stars. Finally the comparison of the observed ICL properties with those predicted from Λ CDM simulations indicates a qualitative agreement and provides insights on the ICL formation. Both observations and simulations indicate that BCG halos and ICL are physically distinct components, with the "hotter" ICL dominating at large radial distances from the BCGs halos as the latter become progressively fainter.

1 Diffuse light in clusters

Deep imaging of massive clusters of galaxies shows that a population of star exists that fills the space among galaxies in clusters. While the indication of its existence came with the early detection by Zwicky in 1951 for the Coma cluster, it was only with the advent of the wide-field cameras equipped with mosaic CCDs that the properties of the clusters' diffuse light, i.e morphology, radial distribution and colors,

Magda Arnaboldi

European Southern Observatory, Garching, Germany, and Obs. of Turin, INAF, Italy

e-mail: marnabol@eso.org

1

were studied in a quantitative way (Uson et al. 1991, Bernstein et al. 1995, Gregg & West 1998, Mihos et al. 2005, Rudick et al. 2010).

Accurate photometric measurements of the diffuse light are difficult to perform because 1) its features are at extremely faint surface brightness of $< 1\%$ of the night sky and 2) it is difficult to disentangle the contribution of the extended outer halos of the brightest cluster galaxies (BCGs) in a cluster core from that of the stars free floating in the cluster potential, i.e. the intracluster light component or ICL. Without the kinematic measurements, the division between BCG halos and ICL is somewhat arbitrary.

Since the discovery of free-floating intracluster planetary nebulae (ICPNs) in the Virgo cluster (Arnaboldi et al. 1996), extensive imaging and spectroscopic observations were carried out to determine their projected phase space distribution, and from it the amount of ICL.

The measurement of the ICL in clusters is relevant from the determination of the barionic fraction condensed in stars, the star formation efficiency and the metal enrichment of the hot intracluster medium, especially in the cluster cores. Because of the long dynamical time across the cluster regions, we expect the distribution function $f(\bar{x},\bar{v})$ of the ICL stars to be different depending on the formation mechanism and its assembly history.

2 PNs as kinematical traces

Planetary Nebulae (PNs) are the late phase of solar-like stars and in stellar populations older than 2 Gyrs one star every few millions is expected to undergo such phase (Buzzoni et al. 2006). Stars in the PN phase can be detected via the relative bright emission in the optical [OIII] line, at λ 5007 Å, because the nebular shell re-emits 10% of the UV photons emitted by the white dwarf at its center in the [OIII] $\lambda 5007$ Å line. When such emission line is detected, the line-of-sight velocity of the PN can be measured via a Gaussian fit.

The number density of PNs trace the light of the parent stellar population. According to the single stellar population theory, the luminosity-specific stellar death rate is independent of the precise star formation history of the associated stellar population (Renzini & Buzzoni 1986). This property is captured in a simple relation such that

$$N_{PN} = \alpha L_{gal} \tag{1}$$

where N_{PN} is the number of all PNs in a stellar population, L_{gal} is the bolometric luminosity of that parent stellar population and α is the luminosity-specific PN number. Predictions from the stellar evolution theory are further supported by the empirical evidence that the PN number density profiles follow light in late- and early-type galaxies (Kimberly et al. 2008, Coccato et al. 2009) and that the luminosity-specific PN number α stays more or less constant for (B-V) color < 0.8, and then decreases

by about a factor 7 for very red (B-V) > 0.8 and old stellar population (Buzzoni et al. 2006).

3 The Virgo cluster core

The presence of diffuse light in the Virgo cluster core is clearly illustrated by the deep image of Mihos et al. (2005), reaching $\mu_v = 28$ mag arcsec^{-2}. It shows a variety of features such as streamers, arcs, plumes and very extended diffuse halos surrounding the large galaxies in the field at surface brightness level of $\mu_v \approx 26.5$ mag arcsec^{-2}, and in the case of M87, with flattened isophotes (c/a=0.5) out to $\sim 37' = 161$ kpc. The different morphologies suggest that we may be seeing several systems superposed along the line-of-sight (LOS) to the Virgo core and their dynamical status may be characterized by a different kinematics.

For the Virgo cluster, there has been considerable success with a two-step approach of identifying PN candidates with narrow-band imaging followed by multi-object spectroscopy. Arnaboldi et al. (1996) observed the outer regions of the giant elliptical M86, measuring velocities for 19 objects. While M86's $v_{sys} = -240$ kms^{-1}, three of these PNs have velocities larger than the mean velocity of the Virgo cluster $\bar{v}_{virgo} = 1100$ kms^{-1}, and turned out to be true ICPNs. Subsequently, 23 PNs were detected in a spectroscopic survey[1] with 2dF on the 4m Anglo- Australian Telescope (Freeman et al. 2000, Arnaboldi et al. 2002). The first confirmation based on detecting the [OIII] doublet in a single PN spectrum was made in Arnaboldi et al. (2003). Since then, Arnaboldi et al. (2004, A04) began a campaign to systematically survey PN candidates in the Virgo cluster using multi-object spectroscopy with the FLAMES/GIRAFFE spectrograph on the VLT. A04 presented the first measurements of the velocity distribution of PNs from three survey fields in the Virgo cluster core and concluded that in two of these fields the light is dominated by the extended halos of the nearby giant elliptical galaxies, while the ICL component dominates the diffuse light in only one field, where a "broad" line-of-sight velocity distribution is measured, and all PNs are true "ICPNs".

The A04 sample was further enlarged with the PN spectra obtained with FLAMES at the ESO VLT by Doherty et al. (2009, D09), and Fig. 1 shows the overview of all the fields in the Virgo cluster core studied thus far.

---

[1] These results were all based on single line identifications, although the second oxygen line was seen with the right ratio in the composite spectrum of 23 PNs observed by Freeman et al. (2000).
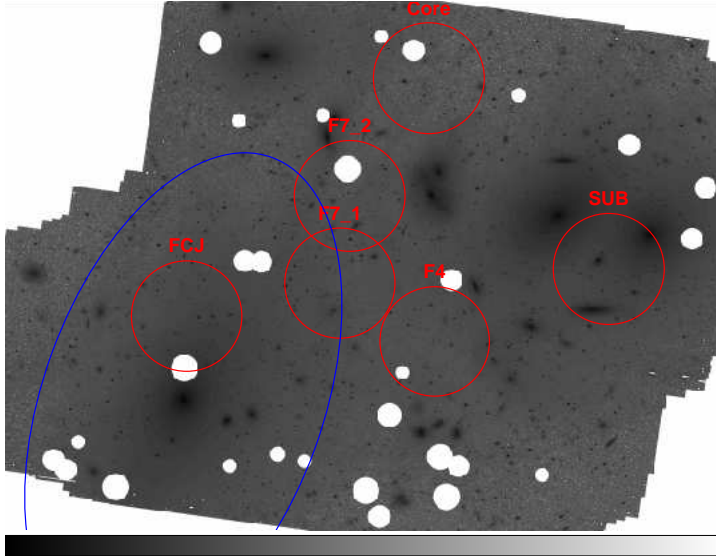
Fig. 1 Deep image of the Virgo cluster core showing the diffuse light distribution (Mihos et al. 2005), with the target fields of A04 and D09 indicated by red circles. The blue ellipse shows the outer isophotes of the M87 halo according to Kormendy et al. (2009).

3.1 PNs line-of-sight velocity and projected phase-space distributions

On the bases of the PNs' position and v_{LOS} in the Virgo cluster core, one can computed the projected phase-space diagram by plotting the PNs v_{LOS} versus radial distance from the center of M87. In this v_{LOS} vs. *radius* diagram several regions can be identified with very different densities: for projected distances $R < 2400''$ most of the PNs are strongly clustered around the systemic velocity of M87, $v_{sys} = 1307$ kms^{-1}, while at $R > 2400''$ the PN velocities spread widely over a velocity range more typical for the Virgo cluster. From this intracluster region, we see a string of low PN velocities at ≤ 800 kms^{-1} reaching far into the M87 halo. At projected distance $R < 1300''$ there are two of these intracluster PNs at ~ 400 kms^{-1}. The remaining PNs are distributed symmetrically around M87's v_{sys} and have mean velocity 1276 ± 71 kms^{-1} and velocity dispersion $\sigma = 247$ kms^{-1} (A04). At $R \sim 2000''$, five PNs are tightly clustered around $v_{sys} = 1307$ kms^{-1}; these have mean velocity 1297 ± 35 kms^{-1} and an rms dispersion of 78 kms^{-1} (D09). At comparable radii there are two additional PNs with velocities of 753 and 634 kms^{-1}; compared to the previous five, these are 7σ and $8\,\sigma$ outliers. It is unlikely that one or two of these outliers are part of the same (very asymmetric) distribution as the five PNs clustered

around M87's v_{sys}[2]. By contrast, they fit naturally into the stream leading from a distance of $1300''$ from the M87 center all the way into the ICL.
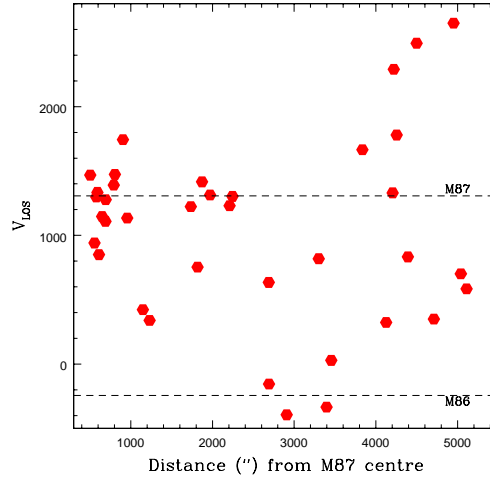

Fig. 2 Distribution of v_{LOS} versus projected distance from the center of M87 for all spectroscopically confirmed PNs in the Virgo core. From D09.

The PNs bound to the M87 halo are then only those ones which are clustered around the systemic velocity of M87. These are confined to radii $R < 2400''$. Outside $R = 2400''$ in Fig. 2 the PNs have larger relative velocities with respect to M87's v_{sys}, with an approximately uniform distribution in the range -300 to -2600 kms^{-1}. Those in the radial range $2400'' < R < 3600''$ are confined to negative velocities with respect to M87, indicating that the ICL component is not phase-mixed yet. These are probably encroaching stars from M86 and other Virgo components. By contrast, the PNs further than $3600''$ from M87 show a broad distribution of velocities, more characteristic of the cluster as a whole.

The ICL PNs show up as approximately flat velocity distribution (VD) besides the peak of velocities from PNs bound to M87. A flat distribution of velocities in addition to the peak near M87's systemic velocity is also seen in the LOSVD of the dwarf spheroidal galaxies in the same region of the Virgo cluster core (Binggeli et al. 1993). However, for the dwarf galaxies the broad velocity distribution extends to significantly more red-shifted velocities, indicating that the dwarfs and ICL PNs kinematics can only partially be related.

In Figure 3 we plot the PNs' positions and those of the dwarfs' in the cluster core. Those PNs in the densest part of the projected phase space diagram are spatially associated with the halo of M87, and they are segregated in radii within $R < 161$

---

[2] The probability of finding 5 PNs with velocity dispersion less than 80kms^{-1} from a Gaussian velocity distribution with $\sigma = 250$ kms^{-1} around $\bar{v} = 1300$ kms^{-1} as measured at 60 kpc is less than 1%.
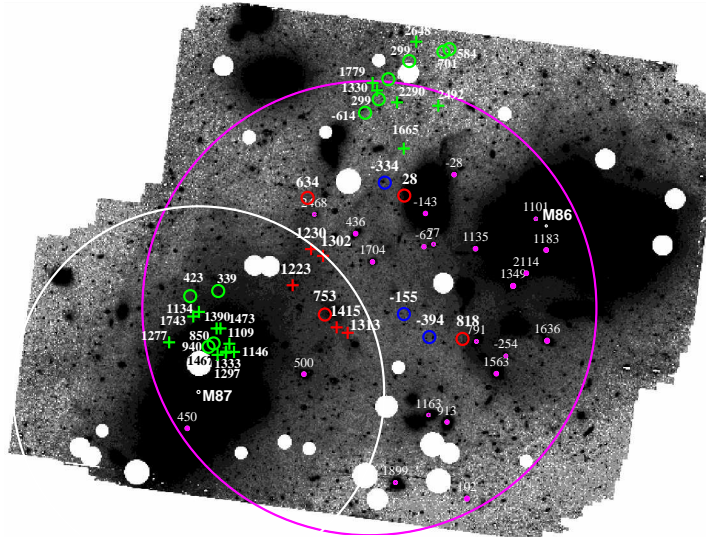
Fig. 3 Deep image of the Virgo cluster core showing the distribution of the intracluster light (from Mihos et al. 2005). The spatial distribution of the spectroscopically confirmed PNs are overlaid. The A04 targets are shown in green; D09 targets are shown in red if red-shifted with respect to Earth and blue if blue shifted. Objects with velocities higher than the mean velocity of Virgo (1100 km s^{-1}) are shown as crosses and those with lower velocities shown as circles. Dwarf spheroidals are marked as magenta dots. The velocities (in km s^{-1}) are labeled for all objects shown. The nominal "edge" of the M 87 halo at $\approx$160 kpc is indicated with a white circle. The pink circle has a 1.5 degree diameter and is centered on the projected midpoint of M87 and M86. North is up and East is to the left. From D09.

kpc, while the ICPNs are scattered across the whole core region, including the M87 halo.

3.2 Dynamical status of the Virgo cluster core

The LOSVD of dwarf spheroidals (dE+dS0) in a 2° radius circular region centered on M87 is very flat and broad, with the peak of the distribution at 1300 kms^{-1} and a long tail of negative velocities (Binggeli et al. 1993). The LOSVD of the ICPNs now confirms that this asymmetry is also present in the very center of the Virgo core, in a 1° diameter region. The projected phase-space diagram of Fig. 2 shows that velocities near the systemic velocity of M86 are seen to about half-way from M86 to M87. The asymmetry and skewness of the LOSVD may arise from the merging of sub-clusters along the LOS (Schindler & Boehringer 1993). In a merging of two clusters of unequal mass, the LOSVD is highly asymmetric with a long tail on one side and a cut-off on the other side, shortly ($\sim 10^9$ yr) before the clusters merge. The observed LOSVDs of the PNs, GCs (Côté et al. 2001), and (dE+dS0) in the Virgo

core can be interpreted as evidence that the two massive sub-clusters in the Virgo core associated with the giant ellipticals M87 and M86 are currently falling towards each other - more or less along the LOS, with M87 falling backwards from the front and M86 forwards from the back - and will eventually merge, i.e. the entire core of the Virgo cluster must then be out of virial equilibrium and dynamically evolving.

What is the relative distance between M87 and M86? Do their halos already touch each other, or are they just before their close pass? PNLF distances (Jacoby et al. 1990) and ground-based surface brightness fluctuation distances indicate that M86 is behind M87 by just under ~ 0.15 mag. However, the most recent surface brightness fluctuation measurements find that M87 and M86 are only at very slightly different distances. Within the errors, the distance moduli (M87: 31.18 ± 0.07, M86: 31.13 ± 0.07) are consistent with being either at the same distance or separated by 1-2 Mpc. Unfortunately the evidence from the relative relative distances of M87/M86 is not conclusive at this stage.

3.3 ICL Large scale distribution in the Virgo cluster from PNs narrow band surveys

Several studies investigated the properties of the ICL in the core of the nearby Virgo cluster by mapping the number density distribution of ICPNs. Expanding on the earlier narrow band imaging work in the Virgo cluster core (Arnaboldi et al. 2002, 2003; Feldmeier et al. 1998, 2003, 2004; Okamura et al. 2002; Aguerri et al. 2005), Castro-Rodriguéz et al. (2009) completed a survey campaign of the ICL distribution at larger scales, outside the Virgo cluster core. In total, they covered more than 3 square degrees in Virgo, at eleven different positions in the cluster and at distances between 80 arcmin and some 100 arcmin from the Virgo core. In several of these regions, the ICL is at least two magnitudes fainter than in the core.

The diffuse light observed in the core of a galaxy cluster contains several luminous stellar components that add up along the LOS to the cluster center: the extended faint halos of the brightest galaxies and the ICL contribution. When computing the ICL fraction in the Virgo core, the surface brightness measurements must then be corrected for the fraction of stars bound to the extended galaxy halos. When one selects only true ICPNs, Castro-Rodriguéz et al. (2009) measure a surface brightness for the ICL of about $\mu_B = 28.8 - 29.5$ mag arcsec^{-2} in the Virgo core and these surface brightness values are consistent with those inferred from the detection of IC RGB stars (Williams et al. 2007).

The comprehensive summary of all surface brightness measurements in Fig. 4 based on ICPN number counts indicates that most of the diffuse light is detected in fields located in the core, within a distance of about 80 arcmin, ≈ 350 kpc, from M87. Outside the core, the mean surface brightness decreases sharply, and the ICL is confined within isolated pointings.

Diffuse stellar light is also measured in sub-structures, around M49 and in the M60/M59 sub-group. The fields F04-2 and F04-6 from Feldmeier et al. (2004) are
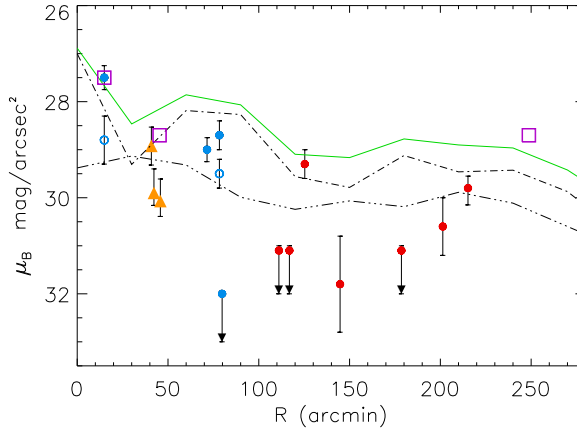
Fig. 4 Surface brightness measurement of diffuse light in the Virgo fields (points) compared with the surface brightness profile of the Virgo galaxies averaged in annuli (lines); radial distances are computed with respect to M87. The green line represents the radial surface brightness profile from light in Virgo galaxies from Binggeli et al. (1987). The dotted-dashed and double dotted-dashed lines correspond to the surface brightness profile associated with giants and dwarf galaxies, respectively. The full blue dots show the surface brightness measurements in the Virgo core fields using ICPNs. The open circles indicate the ICL surface brightness computed from true ICPNs, i.e. PNs not bound to galaxy halos. The triangles represent the surface brightness of the ICL based on IC RGB star counts (see Williams et al. (2007) and the reference therein). The full red dots show the surface brightness measurements outside the Virgo core fields using ICPNs. The arrows indicate the upper limits for the measurements of PNs at certain field positions. The magenta open squares indicate the surface brightness average values μ_B at 15, 50 and 240 arcmin based on the measurements from Feldmeier et al. (2004) data; the measurements at 240 arcmin (F04-2 and F04-6) are close to M49. Radial distances are computed with respect to M87. From Castro-Rodriguéz et al. (2009).

situated in the outer regions of M49, at about 150 kpc from the galaxy center. These fields may contain PNs from the halo of M49 and those associated with the ICL component, which may have formed within sub-clumpB of the Virgo cluster. Because the spectroscopic follow-up in not yet available for these PN candidates, we cannot quantify the fraction of light in the M49 halo and ICL for these fields.

The result for the ICL being more centrally concentrated than the galaxies in the Virgo cluster is confirmed generally for clusters with central BCGs. It agrees with statistical observations of intermediate redshift clusters (Zibetti et al. 2005) and their diffuse light radial profiles.

4 Observing techniques for the kinematics of diffuse light in clusters

In this section we present a short overview of the observing techniques that allow studies of the kinematic of the diffuse light in clusters far beyond 15 Mpc, and explore distant clusters out to Coma, at 100 Mpc. A number of techniques have been developed recently that allow detection and velocity measurements of PNs in the same observing run. We refer to the work of Méndez et al. (2001), which used a sequence of narrow plus broad band images, followed by the dispersed image of the same field. This technique has been applied to NGC 4967 in Virgo and to NGC 1344 in Fornax. The PN Spectrograph (PN.S) is an instrument on the William Herschel Telescope dedicated to measuring PN velocities in nearby galaxies (Douglas et al. 2002). The pupil is split in half before being dispersed in opposite directions in twin spectrographs. A combination of the two exposures allows the identification of emission-line objects and their velocity measurements from the separation between positions in two spectral images.

4.1 Counter Dispersed Slitless Imaging technique

The counter dispersed slitless technique (CDI) used by McNeil et al. (2010) uses only two exposures for each field to obtain positions and velocities of PNs for the cD galaxy NGC 1399, in the Fornax cluster, at D=17 Mpc distance. The field is observed with a dispersed image through a narrow band filter centered at the red-shifted emission of the PN at the systemic velocity of the galaxy being studied. Next the spectrograph is rotated 180 degrees and the same field is exposed again, this time with the dispersion in the opposite direction. As in the PN.S observations, the velocity is a function of the separation between the position of the PN in the two frames. In this way, the slitless technique avoids the two stage selection and measurement process. Because there are no slits or fibers, the light loss is reduced. The number of measurable PN velocities is not limited either by the number of available fibers or the restrictive geometry of the slit. For a comprehensive presentation of the CDI technique and the calibration procedure to derive relative and absolute velocity, and sky position of the emission line sources we refer the reader to McNeil et al. (2010).

4.2 The Multi-Slit-Imaging-Spectroscopy technique

For the PNs in distant galaxies $D > 20$ Mpc, the flux in the [OIII] λ 5007Å emission becomes of the same order as the sky noise in a $30 - 40$ Å wide filter, therefore we need to deploy a technique which substantially reduced the noise in the background sky to be able to detect them. Observing the entire field through slits, a narrow band

filter and a dispersing element significantly reduces the signal from the sky, because we limit it to few Å only. The Multi slit Imaging Spectroscopy (MSIS) technique pioneered at the 8.2 m Subaru telescope and FOCAS spectrograph (Gerhard et al. 2005) involves a grid of slits that are stepped until the entire field has been spectrally imaged through a narrow band filter and a grism. It is a blind technique and spectra are obtained for all the emission line objects that happen to lie beyond the slits. These type of observations detected sample of intracluster PNs in the Hydra (Ventimiglia et al. 2008) and in the Coma cluster (Gerhard et al. 2005, Arnaboldi et al. 2007).

5 The un-mixed kinematics of the intracluster stars in the Fornax and Hydra cluster cores

In this section we provide a concise overview of the most recent results on the un-mixed kinematics of intracluster stars based on PNs velocities in the cores of the Fornax and Hydra clusters, from the works of McNeil et al. (2010) and Ventimiglia et al. (2010, in prep.).

The Fornax cluster and NGC 1399 - Using the CDI technique with the FORS1 spectrograph at the ESO VLT, Mc. Neil et al. (2010) discovered 187 PNs around NGC 1399, the cD galaxy in the Fornax cluster. Data were extracted from a mosaic of 5 fields, which included also the nearby galaxy NGC 1404. Each PN was further classified on the basis the light contribution from the two galaxies at its position, and the difference between the PN velocity and the systemic velocities of NGC 1399 ($v_{sys} = 1425$ kms^{-1}; from NED) and NGC 1404 ($v_{sys} = 1917$ kms^{-1}; from NED). This procedure identified 146 PN associated with NGC 1399, 23 PNs associated with NGC 1404, while 6 PNs were unassigned. The projected PNs phase space distribution v_{LOS} vs. radius in the NGC 1399 surveyed regions indicated the presence of a kinematic component at low velocity $v_{mean} = 800$ kms^{-1} also, in addition to the PN population of NGC 1399 and NGC 1404. A total of 12 PNs are associated with the low velocity component, and they are scattered across the NGC 1399 light distribution, with a concentration in the North-central part. The most recent globular cluster work also show a sample of low velocity objects at similar velocity (Schulbert et al. 2010) which independently support the reality of this substructure.

The presence of a velocity sub-component in the PNs sample superposed on a PN population bound to the NGC 1399 halo indicate the presence of a heterogeneous population including stars left over from previous accretion, merger or tidal stripping events; these stars are still in the process of phase-mixing.

The Hydra cluster and NGC 3311 - Ventimiglia et al. (2010, in prep.) performed MSIS observations with FORS2 at the ESO VLT of the core region of the Hydra cluster, centered on its cD galaxy NGC 3311. They detected a total of 56 PNs in a single field of 100×100 kpc^2 , and analyzed their velocity field. The PNs LOSVD in this region follows a multi-peaked distribution, see Figure 5: in addition to a broad symmetric component centered at the systemic velocity of the cluster ($v_{hydra} = 3683$

kms^{-1}), two narrow peaks are detected at 1800 kms^{-1} and 5000 kms^{-1}. These secondary peaks unmask the presence of un-mixed stellar populations in the Hydra core.

The spatial distribution of the PNs associated with the narrow velocity sub-component at 5000 kms^{-1} is superposed and concentrated on an excess of light in the North-East quadrant of NGC 3311, as detected from the 2 dimensional light decomposition of the NGC 3311/NGC 3309 B band photometry. On the same sky position we detect a group of dwarf galaxies with $v_{LOS} \approx 5000$ kms^{-1}. Deep long-slit spectra obtained at the position of the dwarf galaxy HCC26 situated at the center of the light excess show absorption line features from both HCC26 and the light excess which are consistent with v_{LOS} of about 5000 kms^{-1} (Ventimiglia et al. 2010). We conclude that the PNs in the 5000 kms^{-1} sub-component, the dwarfs galaxies and the light excess in the North-East quadrant of NGC 3311 occupy the same region of the phase space, and are physically associated.

Also in the case of the relaxed Hydra-I cluster, PN kinematics, photometry and deep absorption spectra support the evidence for an accretion event whose stars are being added to both the cluster core and the halo of NGC 3311.

Fig. 5 The PNs LOSVD in the core of the Hydra cluster obtained from the MSIS observations by Ventimiglia et al. (2010). The LOSVD is shown by the black line, while the blue and red curves indicate the measured transmission curves of the narrow band filters used to cover the Hydra velocities; the normalization is arbitrary. The magenta, green and gray vertical lines indicate the systemic velocity of the Hydra-I cluster, NGC 3311 and NGC 3309, respectively.
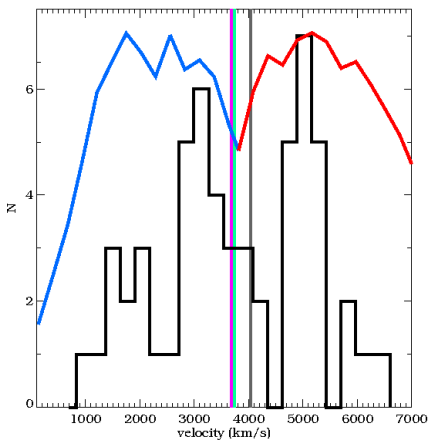
6 The on-going sub-cluster merger in the Coma cluster core

The Coma cluster is the richest and most compact of the nearby clusters, yet there is growing evidence that its formation is still on-going. A sensitive probe of this evolution is the dynamics of intracluster stars, which are unbound from galaxies while the cluster forms, according to cosmological simulations. With the MSIS technique Gerhard et al. (2005) detected and measured the v_{LOS} of 37 ICPNs associated with the diffuse stellar population of stars in the Coma cluster core, at 100 Mpc distance.

These are the most distance singles stars whose spectra have been acquired in addition to cosmological supernovae stars. Gerhard et al. (2007) detected clear velocity sub-structures within a 6 arcmin diameter field centered at $\alpha(J2000) = 12:59:41.8; \delta(J2000)27:53:25.4$, nearly coincident with the field observed by Bernstein et al. (1995) and ~ 5 arcmin away from the cD galaxy NGC 4874. A sub-structure is present at ~ 5000 km s^{-1}, probably from in-fall of a galaxy group, while the main intracluster stellar component is centered around $\sim$6500 km s^{-1}, $\sim$700 km s^{-1} offset from the nearby cD galaxy NGC 4874 ($v_{sys} = 7224$ km s^{-1}; from NED) . The kinematics and the elongated morphology of the intracluster stars (Thuan & Kormendy 1977) show that the cluster core is in a highly dynamically evolving state. In combination with galaxy redshift and X-ray data, this argues strongly that the cluster is currently in the midst of a sub-cluster merger. The NGC 4889 sub-cluster is likely to have fallen into Coma from the eastern A2199 filament, in a direction nearly in the plane of the sky, meeting the NGC 4874 sub-cluster arriving from the west. The two inner sub-cluster cores are presently beyond their first and second close passage, during which the elongated distribution of diffuse light has been created. Gerhard et al. (2007) also predict the kinematic signature expected in this scenario, and argue that the extended western X-ray arc recently discovered traces the arc shock generated by the collision between the two sub-cluster gas halos.

7 Cosmological simulations and ICL

The predicted spatially averaged radial distribution of ICL from recent high resolution hydrodynamical simulations of cluster formation in Λ CDM universe (Murante et al. 2004) is in broad agreement with the observed radial profiles for the ICL in clusters. Furthermore predictions from these simulations that the largest portion of the ICL is formed during the assembly of the most luminous cluster galaxies (Rudick et al. 2006, Murante et al. 2007) is supported by the observed ongoing mergers in Coma and Virgo cores, and by the presence of ICL around sub-clusters/groups.

Quantitative analysis of the ICL kinematic from cosmological simulations is on-going (Coccato et al. 2010, in prep). Studies of the galaxy halo and ICL particles in cosmological simulations (Dolag et al. 2010) further support the physical distinction between the central BCG and the ICL component in clusters.

8 Summary and Conclusions

The kinematics of the ICL provide unique information to asses the dynamical status of the nearby cluster cores:

- In the Virgo cluster, M87 and the M86/M84 sub-clusters are approaching along the LOS and they are currently before their first close passage.

- In the Coma cluster, the elongated morphology and kinematics of the ICL, the galaxy morphology and X-ray data are consistent with the merging of NGC 4889 and NGC 4874 along a binary orbit, the two galaxies being currently observed beyond their first and second close passage.
- the Hydra and Fornax clusters show evidence for un-mixed stellar components coming from accretion/tidal stripping events in their cores.

The superposition of the various kinematic components underscores the complexity of velocity measurements in cluster cores and the necessity of using discrete tracers to detect these components. In all cases the kinematical data indicate that the galaxy halos and ICL are discrete components; and the former do not blend continuously in the latter. The evidence for merging (in Coma) and accretion indicates that the build up of the ICL is an on-going process.

References

. Aguerri, M., et al. 2005, AJ, 457, 771
. Arnaboldi, M., et al. 1996, ApJ, 472, 145
. Arnaboldi, M., et al. 2002, AJ, 123, 760
. Arnaboldi, M., et al. 2003, AJ, 125, 514
. Arnaboldi, M., et al. 2004, ApJ, 614, L33 (A04)
. Arnaboldi, M., et al. 2007, PASJ, 59, 419
. Bernstein, G.M., et al. 1995, AJ, 110, 1507
. Binggeli, B., Tammann G.A., Sandage, A. 1987, AJ, 94, 251
. Binggeli, B., Popescu, C.C., Tammann, G.A. 1993, A&AS, 98, 275
. Buzzoni, A., Arnaboldi, M., & Corradi, R.L.M. 2006, MNRAS, 368, 877
. Castro-Rodriguéz, N., et al. 2009, A&A, 507, 621
. Coccato, L. et al. 2009, MNRAS, 394, 1249
. Côté, P., et al. 2001, ApJ, 559, 828
. Doherty, M., et al. 2009, A&A, 502, 771 (D09)
. Dolag, K. et al. 2010, MNRAS, 405, 1544
. Douglas, N., et al. 2002, PASP, 114, 1234
. Feldmeier, J.J., et al. 1998, ApJ, 503, 109
. Feldmeier, J.J., et al. 2003, ApJS, 145, 65
. Feldmeier, J.J., et al. 2004, ApJ, 615, 196
. Freeman, K.C., et al. 2000, ASP Conf. Ser., 197, 389
. Gerhard, O., et al. 2005, ApJL, 621, 93
. Gerhard, O., et al. 2007, A&A, 468, 815
. Gregg, M.D., & West, M., 1998, Nature, 396, 549

.   Jacoby, G., et al. 1990, ApJ, 356, 332
.   Kormendy, J. et al. 2009, ApJS, 182, 216
.   Kimberly, H.A, et al. 2008, ApJ, 683, 630
.   McNeil, E.K., et al. 2010, A&A, 518, 44
.   Méndez, R.H., et al. 2001, ApJ, 563, 135
.   Mihos, J.C., et al. 2005, ApJL, 631, 41
.   Murante, G., et al. 2004, ApJL, 607, 83
.   Murante, G., et al. 2007, MNRAS, 377, 2
.   Okamura, S., et al. 2002, PASJ, 54, 883
.   Renzini, A. , Buzzoni, A., 1986, in Chiosi C., Renzini A., eds., Spectral Evolution of Galaxies.
    Reidel, Dordrecht, p. 195
.   Rudick, C.S., et al. 2006, ApJ, 648, 936
.   Rudick, C.S., et al. 2010, ApJ, 720, 569
.   Schindler, S., & Boehringer, H. 1993, A&A, 269, 83
.   Schuberth, Y., et al. 2010, A&A, 513, 52
.   Thuan, T.X., & Kormendy, J. 1977, PASP, 89, 466
.   Uson, J.M., et al. 1991, ApJ, 369, 46
.   Ventimiglia, G., Arnaboldi, M., & Gerhard, O. 2008, Astronomische Nachrichten, MNRAS,
    329, 1057
.   Zibetti, S., et al. 2005, MNRAS, 358, 949
.   Williams, B.F., et al. 2007, ApJ, 654, 835